Int. J. Electrochem. Sci., 14 **(2019)** 10538 – 10564, doi: 10.20964/2019.11.51

International Journal of
ELECTROCHEMICAL
SCIENCE
www.electrochemsci.org

Treatment of Aqueous Selenocyanate Anions Using Electrocoagulation

Taye Saheed Kazeem, Bashir Alhaji Labaran, Habib-ur-Rehman Ahmed, Tariq Mohammed, Mohammed Hussain Essa, Mohammad Saleh Al-Suwaiyan, Muhammad Shariq Vohra[*]

Civil and Environmental Engineering Department, King Fahd University of Petroleum & Minerals, Dhahran, Saudi Arabia
[*]E-mail: vohra@kfupm.edu.sa

Received: 2 August 2019 / *Accepted:* 13 Sepyember 2019 / *Published:* 7 October 2019

This study removed selenocyanate anions ($SeCN^-$) from synthetic wastewater using a lab-scale batch electrocoagulation (EC) process. $SeCN^-$ removal increased with an increase in the applied current (0.4-1.2 A) and EC time (up to 8 hrs) but reduced with an increase in the initial concentration (10-50 mg/L) and pH (4-8). The $SeCN^-$ species was initially oxidized to selenite (SeO_3^{2-}) and selenate (SeO_4^{2-}), which were then adsorbed onto iron hydroxide or aluminium hydroxide sludge produced from Fe or Al ions released at the anode. This was confirmed by the periodic analysis of water samples from the reactor and the characterization studies done on the sludge, including SEM and EDX. The glassy carbon and graphite electrodes only oxidized selenocyanate anions to selenite and selenate without forming precipitants for adsorption of these Se species. The zeta potential results for steel electrodes showed that surface charge of sludge changed from positive at low pH (pH 4) to negative at high pH (pH 8) thus negatively influencing the adsorption of selenium species. The SEM/EDX results explained the superior adsorption capacity of iron hydroxide compared to aluminium hydroxide. Molecular level simulation results indicated that the van der Waals cohesive energy density (CED) supports the higher removal efficiency of steel electrodes for selenium species in comparison to aluminium electrodes.

Keywords: Electrocoagulation, Selenocyanate anions, Selenite, Selenate, Molecular simulation

1. INTRODUCTION

Selenium in nature typically occurs in four oxidation states: elemental selenium (Se^0), selenide (Se^{2-}), selenite (SeO_3^{2-}) and selenate (SeO_4^{2-}) [1]. Although it is an essential nutrient at trace levels [2], higher selenium intake is detrimental to human health [3]. It is therefore governed by stringent regulations both for drinking water and discharge into the environment. Though selenium in freshwater exists typically as selenite and selenate [4], however, the selenocyanate anions ($SeCN^-$) have also been

found in wastewaters from oil refining industries [5, 6] and mining operations [7, 8]. The toxic selenocyanate anions are produced in respective aqueous streams due to combination of elemental selenium (Se^0) with free cyanide (CN^-) [9]. Also, a biological pathway for its occurrence is the conversion of selenium present in the surface water by green algae [10].

The selenocyanate anions are highly soluble and therefore very mobile form of selenium[7]. Considering this, several methods have been studied for treating aqueous selenium, including precipitation with metal oxides such as iron, copper and tin [1, 11], ion exchange, and bioremediation [7, 12, 13], photocatalytic degradation [14-16], adsorption [17] and electrocoagulation [2, 18]. The effectiveness of a specific technology is dependent on several process parameters including concentration, speciation, and pH [2, 11]. However, selenocyanate anions treatment is more challenging compared to the other selenium species due to difficulty in breaking down the $SeCN^-$ complex and also because of its low adsorption [5]. Though biological treatment has been shown to convert selenocyanate anions to selenite and selenate, however it requires further treatment [5]. The photocatalytic degradation has shown promise in terms of conversion of selenocyanate anions to selenite and selenite followed by their reduction to elemental selenium using hole scavengers such as EDTA [14] and removal via precipitation [18]. Direct precipitation with the zerovalent iron (Fe^0) [5] and copper [11] has also been successfully applied to selenocyanate anions from aqueous phase via forming elemental selenium. These studies indicate that an effective solution for selenocyanate anions treatment could be a two-step process wherein the selenocyanate anions are first oxidized to selenite and/or selenate by a specific oxidizing agent, followed by selenite/selenate removal either because of co-precipitation reduction to elemental selenium and/or adsorption. Nevertheless, one of the challenges in this approach is that the oxidation step needs to be controlled so as not to further oxidize selenite to selenate, as selenate does not co-precipitate effectively [5].

The electrocoagulation (EC) process has also been studied as a possible option for selenium removal by Baek et al. [18] using the iron electrode as an anode and the copper electrode as a cathode. It was proposed that selenate was first reduced to selenite and subsequently to either elemental selenium or selenide. Hansen et al. [2] also treated selenium from petroleum wastewater using iron electrodes and a batch airlift reactor. However, the selenium reaction intermediates have not been described therein as well, which does not allow to establish the underlying mechanism involved in the selenium removal. It was also observed that the pH is an important process variable.

Although electrocoagulation (EC) is a promising technique, its application for aqueous selenocyanate anions has not been investigated to the best of our knowledge. The EC process offers the dual advantage of destroying/oxidizing the $SeCN^-$ species, followed by its uptake by the electrocoagulant as produced during the process. The present study, therefore, aims to treat aqueous selenocyanate anions using the EC process using the steel, aluminum, glassy carbon and graphite electrodes. The effects of different electrode materials and process variables are investigated. This study also explores the reaction intermediates produced, along with kinetic modeling and molecular level simulation for improved application and understanding.

2. MATERIALS AND METHODS

2.1. Materials

The reagent grade chemicals used for all experiments included potassium selenocyanate anions (KSeCN, Aldrich, Germany), sodium selenite (Na_2SeO_3, Aldrich, Germany), potassium selenate (K_2SeO_4, Aldrich, Germany), sodium nitrite ($NaNO_2$, Aldrich, Germany), sodium nitrate ($NaNO_3$, BDH, England), sodium cyanide (NaCN, Fisher Scientific, USA), potassium cyanate (KOCN, Aldrich, Germany), ammonium chloride (NH_4Cl, BDH, England), calcium chloride ($CaCl_2.2H_2O$, Fisher Scientific, USA), sodium bicarbonate ($NaHCO_3$, Fisher Scientific, USA), sodium chloride (NaCl, Fisher Scientific, USA), sodium hydroxide (NaOH, BDH, England) and nitric acid (HNO_3, BDH, England). The electrodes used in this study included Steel electrodes (9.5 cm x 5 cm x 0.1 cm), Aluminum electrodes (9.5 cm x 5 cm x 0.1 cm), Graphite electrodes (12 cm x 10 cm x 0.5 cm) and Glassy carbon electrodes (10 cm diameter).

2.2. Reactor Setup

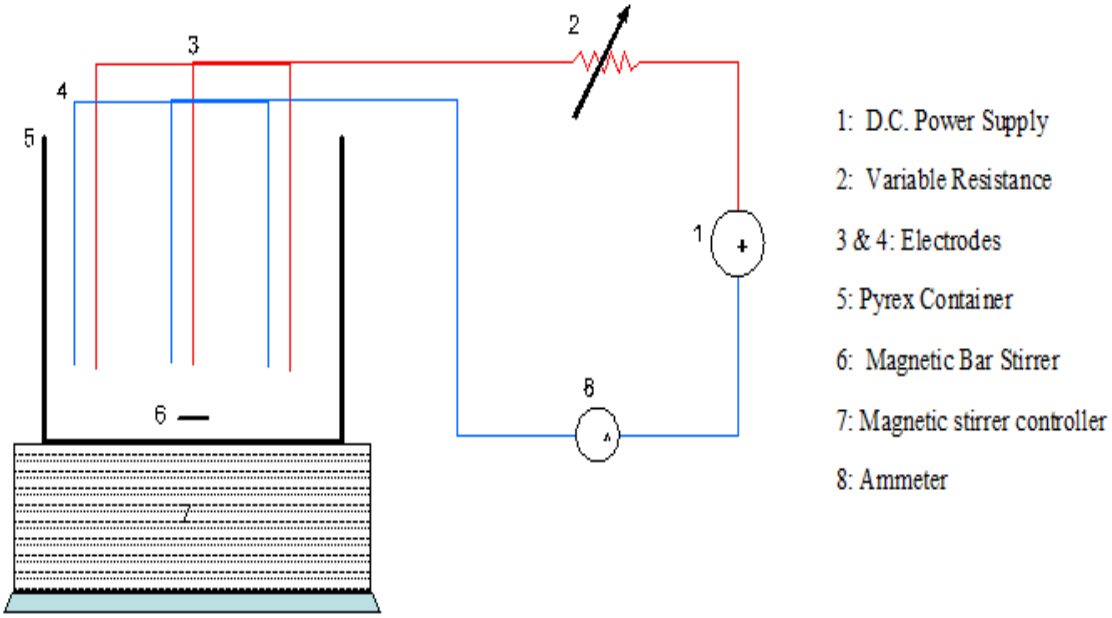

Figure 1. Set-up used for the electrocoagulation experiments

Experiments on electrocoagulation treatment of selenocyanate anions were performed in an electrochemical reactor. **Fig. 1** provides details for the experimental setup used. A beaker of 2 L capacity (Pyrex, USA) was used as the batch reactor. The batches of selenocyanate anions containing water were synthetically prepared using stock solutions of potassium selenocyanate anions, calcium chloride, sodium bicarbonate and sodium chloride along with high purity water (Corning Mega-Pure System, USA). The electrodes were positioned vertically in the beaker containing the synthetic water solution and parallel to each other with an inter-electrode distance of 5 cm (**Fig. 1**). A DC power supply source

(LG, South Korea) was used as a power source to provide current and voltage across the electrodes. The solution was constantly mixed using a magnetic stirrer (Corning, USA) to ensure homogeneity in the reactor. A pH meter (WTW, Germany) was used to monitor pH.

The selenocyanate anion concentrations studied were 10, 30 and 50 mg/L. The initial pH was adjusted using a dilute nitric acid or sodium hydroxide solution and a blank sample was collected before and after the adjustment of pH. After this step the electrocoagulation process was started and samples were collected at specific time intervals, filtered using 0.2 µm filters (Whatman, Germany) and kept in clean vials ready for analysis. At the end of each experiment, the resultant sludge was dried at 50°C and then stored for characterization purpose.

2.3. Analysis

The collected samples were analyzed for selenocyanate anion ($SeCN^-$), selenite (SeO_3^{2-}), selenate (SeO_4^{2-}), cyanide (CN^-), cyanate (OCN^-), ammonium (NH_4^+), nitrite (NO_2^-) and nitrate (NO_3^-) using an advanced ion chromatography system (Metrohm, Switzerland). The respective IC setup was calibrated using standards for each respective species. A Metrosep Anion Dual 2 IC column 4.6 mm x 75 mm (6.1006.100, Metrohm, Switzerland) was used for the analyses of all respective anionic species. The eluent composition for the conductivity detector setup was 1.8 mM Na_2CO_3 and 2 mM $NaHCO_3$ and the eluent flow rate was 0.7 ml/min. VA detector was also used for selenocyanate anions analysis. The eluent composition for the VA detector setup was 100 mM NaOH and the eluent flow rate was 0.7 ml/min. The cationic species were analyzed using Metrosep C4 column 4mm x 250 mm (6.1050.430, Metrohm, Switzerland) and 1.7 mM nitric acid as eluent at a flowrate of 0.9 ml/min. The pH analyses were conducted using a well calibrated pH meter (WTW, Germany).

2.4. Sludge Characterization

The X-Ray Diffraction (XRD) characterization of sludge was completed using a standard X-ray diffractometer (Rigaku, Japan) equipped with Cu Kα radiation (λ = 0.1542 nm) operated at 40 kV and 40 mA with a divergence slit of 5°. The diffraction angle varied from 4° to 80° at a scanning rate of 2°/min. The IR spectra of the sludge samples were determined using a FTIR spectrometer setup (Thermo Scientific, USA). Data was collected by averaging 32 scans, at a resolution of 4 cm^{-1} from 400-4500 cm^{-1}. For SEM analysis, sludge samples were gold coated for 3 minutes to make the surface conductive and the photo images were taken using Field Emission SEM (Tescan, Czech Republic). The same equipment was used for the EDX analysis. The zeta potential were completed using a Malvern Zetasizer Nano-ZS setup (Malvern, USA).

2.5. Molecular Level Simulation

The molecular level simulations were carried out using the Materials Studio software (2013) at the high-performance computing facilities (HPC) at KFUPM. The most important inputs for any molecular simulation scheme are the choice of the representative compounds, formulation of the

representative unit cell with periodic boundary conditions, and the application of a force field to run the appropriate ensemble. After the choice of the various molecules involved, the simulation was performed generally in three steps (**Fig. 2**): sorption of various combinations/proportions of the molecules in a periodic unit cell, geometry optimization using molecular mechanics principles, and determining the cohesive energy density (CED).

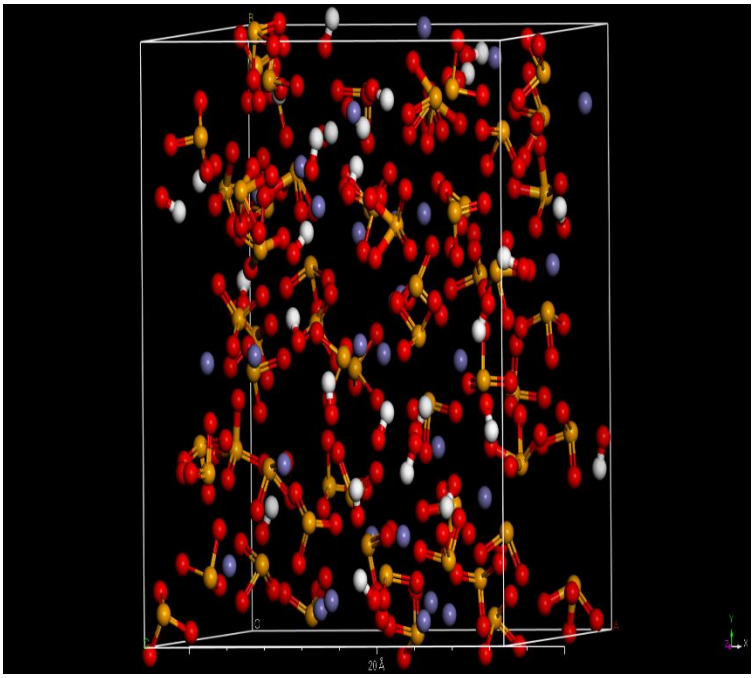

A

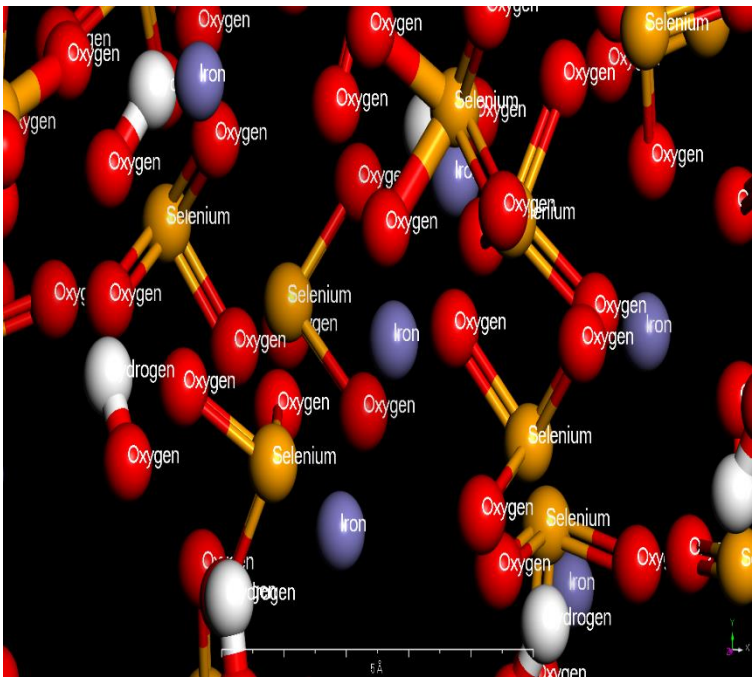

B

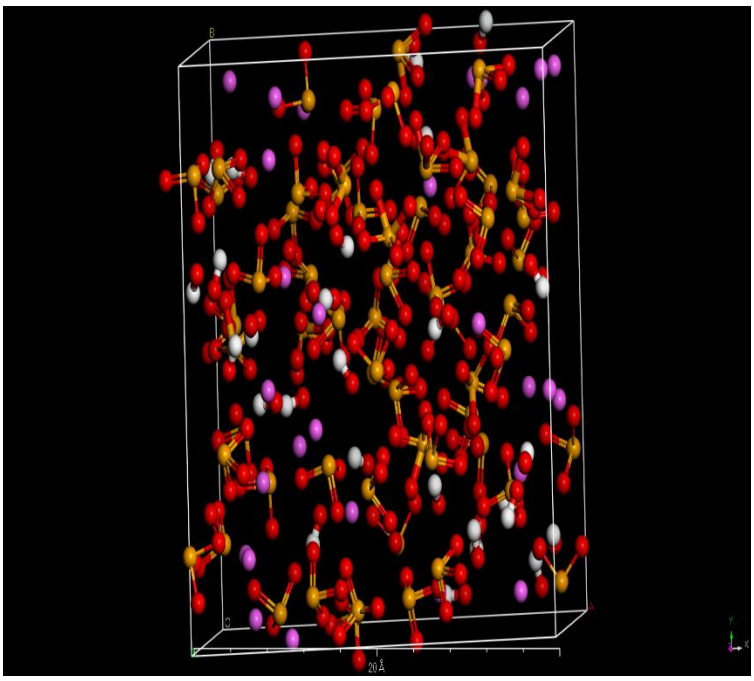

C

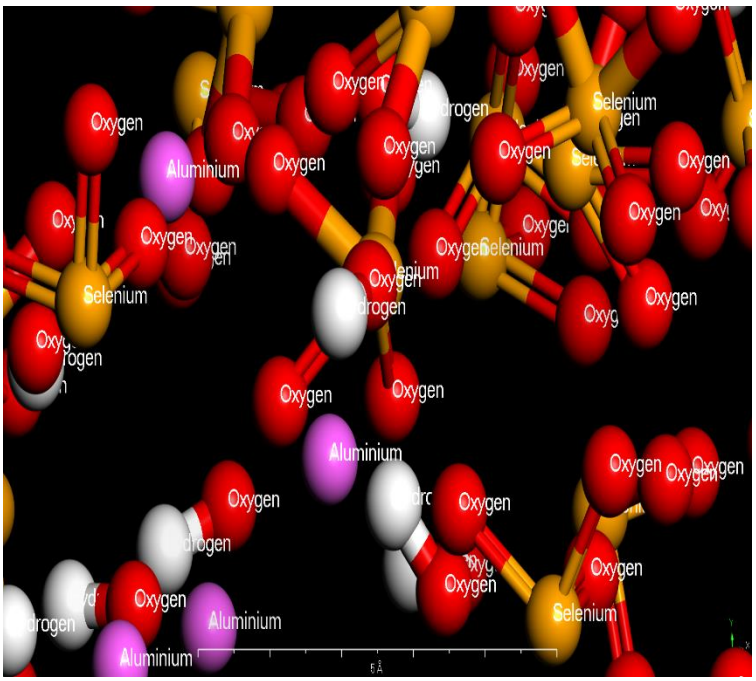

D

Figure 2. Periodic unit cells of the molecular simulations of (a) the interactions of iron hydroxides with the selenium oxides, (b) close-up view of the interactions shown in (a), (c) the interactions of aluminum hydroxides with selenium oxides, and (d) close-up view of the interactions shown in (c)

To simulate the interactions, sorption of the molecules was carried out in a 20Å periodic cubic unit cell. For the simulation purpose, Metropolis Monte Carlo method was selected in the Sorption module of the Materials Studio software. In each sorption step, the molecules occupied spaces in the unit cell to lower the overall energy of the system.

Table 1. Various concentrations of selenite and selenate used in the molecular simulations

Concentration (%)	SeO_3	SeO_4
A	50	50
B	25	75
C	75	25

Maximum possible number of the combination of molecules (Table 1) was sorbed in each 25000 steps, and then the energy of the system was minimized through the use of the Forcite module deploying Molecular Dynamics technique. The Forcite module of the software with the NPT (constant number of particles, pressure, and temperature) ensemble was utilized, and simulations were conducted using a specially designed modified universal force field for 5 to 30 ps in 0.5-fs intervals or till a constant volume was achieved. The Universal Force Field (UFF), one of the force fields in the software has been modified for this research purpose. Several parameters in UFF such as atom types, atom typing rules, diagonal van der Waals, and generators were modified for Na, Ca, Mg, Al, and Si considering the parameters proposed in CLAYFF force field. Maximum time and the unit time interval pertaining to the simulations were adopted considering the achievement of the equilibrium and a stable density at the end of each step of the simulations. Berendsen thermostat and a decay constant of 0.1 ps was adopted to control the temperature in the simulation. During the simulation, the temperature was kept at 298 K. Simulations were conducted with the atmospheric pressure (100 kPa) and a Berendsen barostat with a decay constant of 0.1 ps to control the pressure of the system.

3. RESULT AND DISCUSSION

3.1. Effect of Electrode Type

The effect of electrode type on the removal of $SeCN^-$ from the aqueous system was carried out using the steel, aluminum, graphite, and, glassy carbon electrodes (**Fig. 3 & 4**). The highest and fastest removal was achieved using the steel electrode. Furthermore, though both glassy carbon (**Fig. 3**) and graphite (**Fig. 4**) electrodes caused the destruction of $SeCN^-$ (equation 1) and achieved considerable $SeCN^-$ removal followed by the oxidation to SeO_3^{2-} and SeO_4^{2-}, the respective electrodes did not yield flocs that can serve as an adsorbent and consequently the total selenium remained unchanged during the course of reaction.

$$SeCN^- \longrightarrow Se + CN^- \quad (1)$$

Unlike glassy carbon and graphite, both the steel and aluminum electrodes first oxidized $SeCN^-$ and also removed the reaction products via adsorption onto the formed flocs. Furthermore, at pH 8 (**Fig. 4**), due to a higher adsorption capacity of hydrous ferrous and ferric oxides in comparison to hydrous aluminium oxides, we note higher selenium removal efficiency for the iron based precipitates. Several authors have also previously reported the superior adsorption capacity of hydrous ferrous/ferric oxides

over hydrous aluminum oxides for various anionic water contaminants [19-23]. Hence adsorption seems to play an important role in the electrocoagulation process as also noted previously [18].

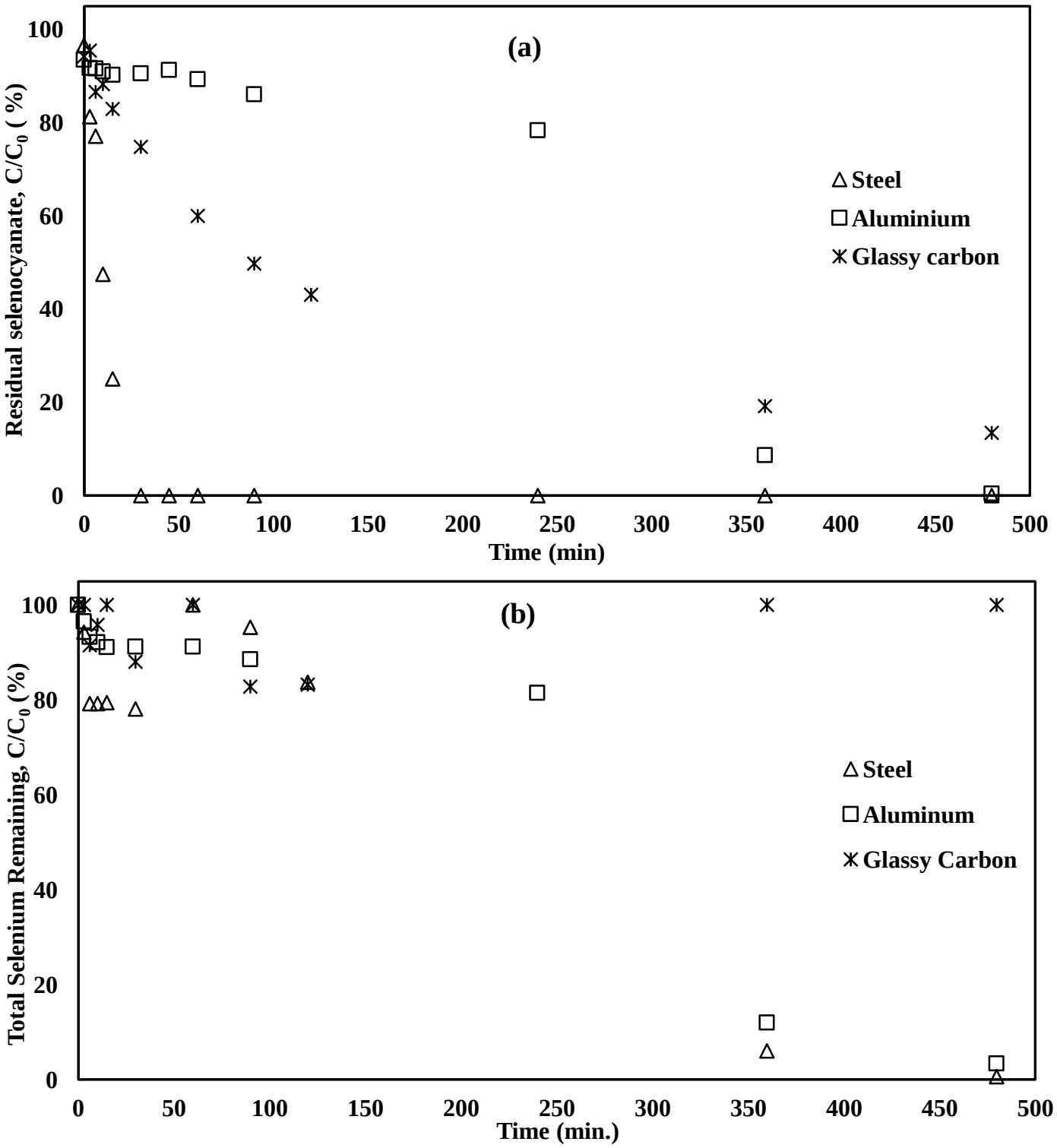

Figure 3. Effect of electrode type on (a) Selenocyanate anions removal, (b) Total Se removal at pH 4, 1.2 A, and 10mg/L.

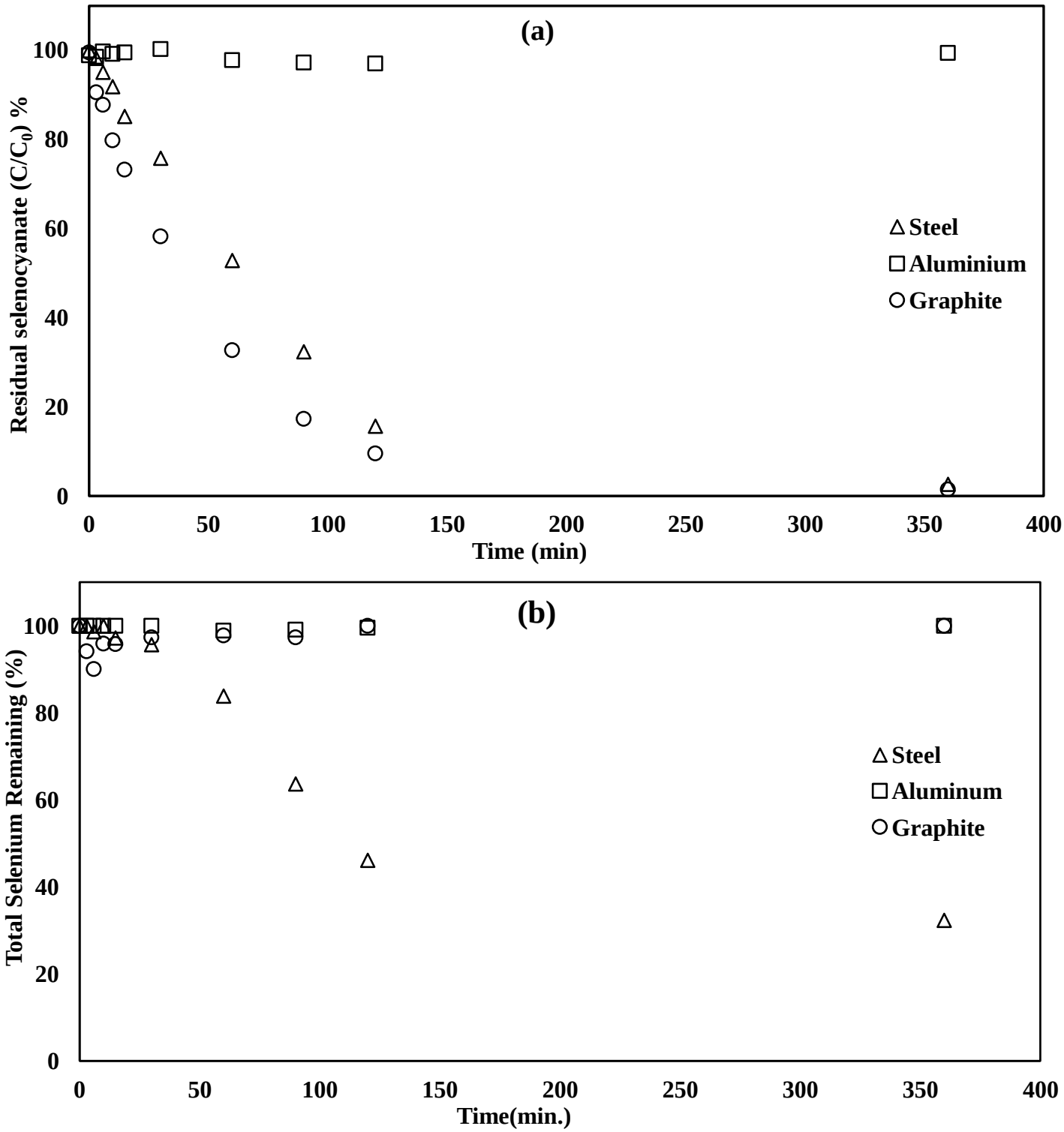

Figure 4. Effect of electrode type on percentage removal of (a) Selenocyanate anions removal, (b) Total Se removal at pH 8, 1.2 A, 50 mg/L.

For example, Kumar et al. [19] noted a far superior removal efficiency for the iron based electrodes compared to the aluminum electrodes for arsenite removal that was suggested to be adsorbed onto the produced metal hydroxides. In another electrocoagulation study the steel electrode was noted to be better than the aluminum electrode [20]. It should also be noted that the classical aqueous speciation

chemistry for the iron based coagulants show a broader optimum precipitation range as compared to the aluminum based precipitation systems, which could also explain the above noted experimental trends.

3.2. Effect of Initial pH

The initial pH has a significant effect on the removal efficiency of the target pollutants as it influences the charge of both adsorbent and adsorbate. The zeta potential (**Fig.5**) values for the steel electrode sludge show a transition from positive at pH 4 to negative at pH 8. It can be noticed from the figure that the point of zero charge occurs at a pH above pH 6 and this observation has been previously reported for ferric oxide to have a pH_{PZC} close to pH 7 [24]. At lower pH (below pH_{PZC}), the surface of the adsorbent is positively charged that stimulated attraction for the anionic species. Beyond the pH_{PZC}, the surface of the adsorbent becomes negative which repels the anionic species.

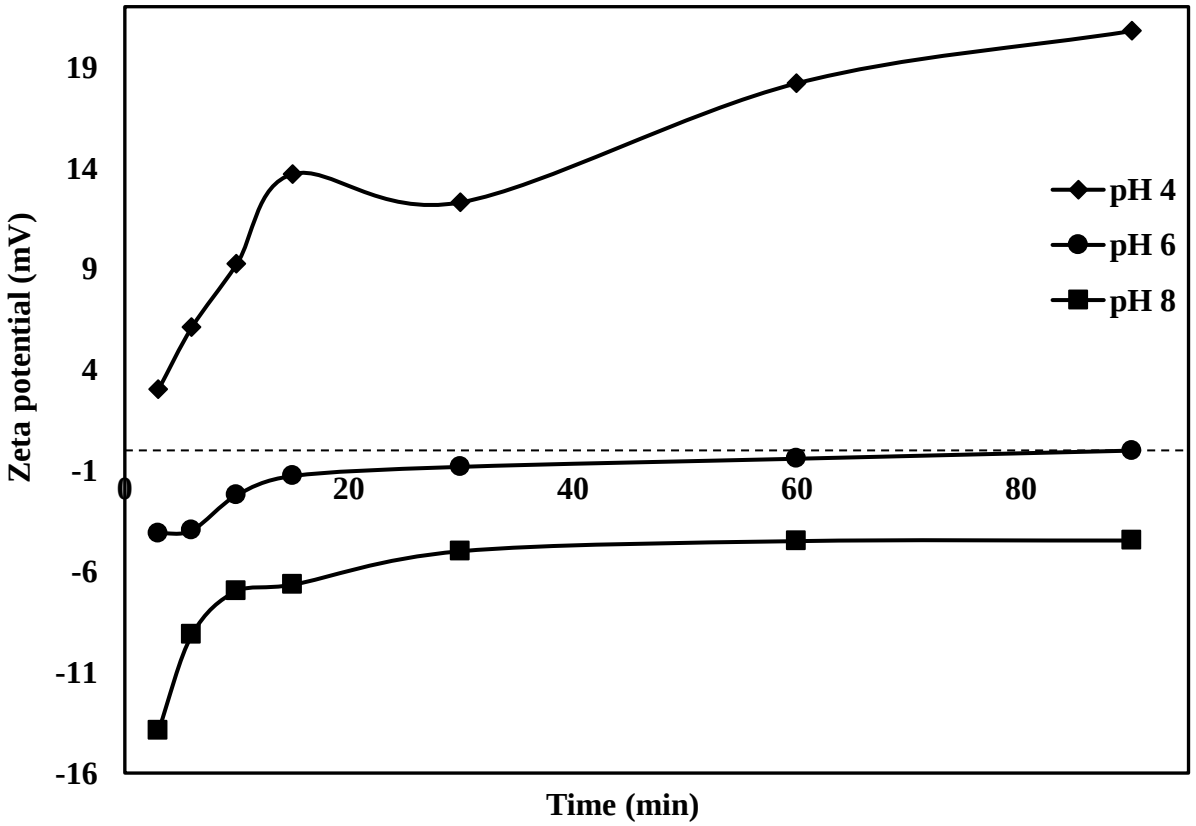

Figure 5. Effect of pH on zeta potential during electrocoagulation of $SeCN^-$ operated at 1.2 A and initial concentration of 50 ppm.

This is seen at the basic conditions (pH 8) in **Fig. 5** that the zeta potential is negative indicating a negative surface charge which is not favorable for adsorption of anionic species. As shown in **Fig. 6 (a & b)**, the percentage removal efficiency of $SeCN^-$ decreases with an increase in pH. Electrostatic interaction between the $SeCN^-$ (as well as SO_3^{2-} and SO_4^{2-}) and the adsorbing surface of the generated flocs yields higher selenium removal efficiency (due to attraction) at low pH and higher removal efficiency transpires at high pH. The selenium species removal at lower pH thus suggests that the surface

of solid will be positively charged (Fig. 5) that will initiate $SeCN^-$ and other selenium species adsorption. A lower $SeCN^-$ removal at higher pH results because of a shift in precipitate/ sludge charge. Nevertheless, $SeCN^-$ removal increases at higher EC times. Labaran and Vohra [15] who studied aqueous phase selenite and selenate removal using the TiO_2 photocatalysis also observed higher selenite/selenate species removal at acidic pH values. The authors discussed different mechanisms and elaborated on the role of positively charged TiO_2 surface below pH_{zpc} that enhanced TiO_2 surface based adsorption and subsequent reduction of respective selenium species. Furthermore, an earlier study [16] that focused on the photocatalytic treatment of selenocyanate anion also reported a larger buildup of selenite species at higher pH values, with less selenite adsorption and less selenate formation. At higher pH adsorption of selenite at the photocatalyst surface was less conducive because of electrostatic repulsion between negatively charged TiO_2 surface ad anionic selenite species. Baek et al. [18] who reported higher ferrous hydroxide formation at higher current during iron anode based electrocoagulation process report adsorption of selenate species onto ferrous hydroxide followed by reduction of former (to elemental selenium or selenide) and oxidation of latter to ferric hydroxide. Furthermore, Meng et al. [5] who investigated removal of selenocyanate anion from an oil refinery effluent employing Fe(0) elemental iron also noted efficient reduction of selenocyanate anion from respective streams at an optimum pH value of 6. The authors using XPS (X-ray photoelectron spectroscopy) results suggested elemental selenium and ferrous selenide formation. Similarly, higher selenium removal efficiency as noted in Fig. 6 can also be explained based on both enhanced adsorption and reduction of surface bound selenium species especially at acidic pH values. In another study using steel and aluminum electrodes, optimum pH of 6 was reported for strontium removal with reduced process noted below and above pH 6 [20].

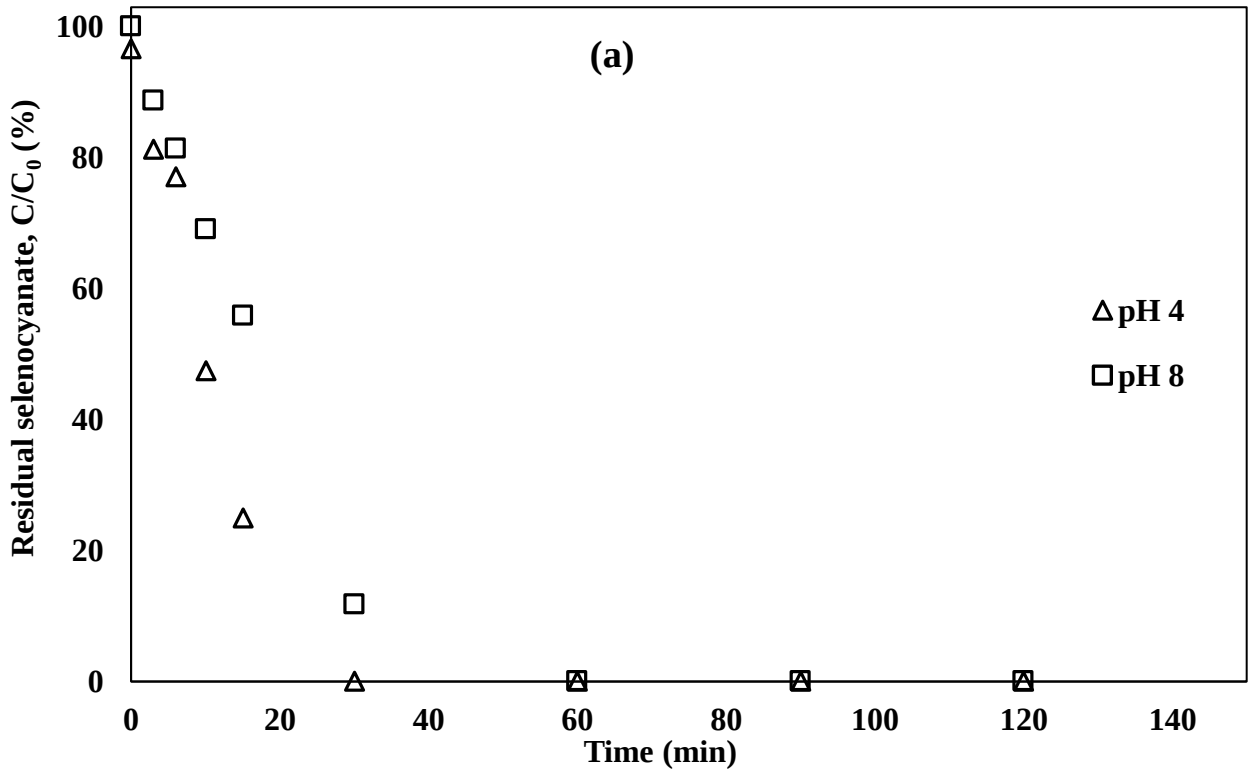

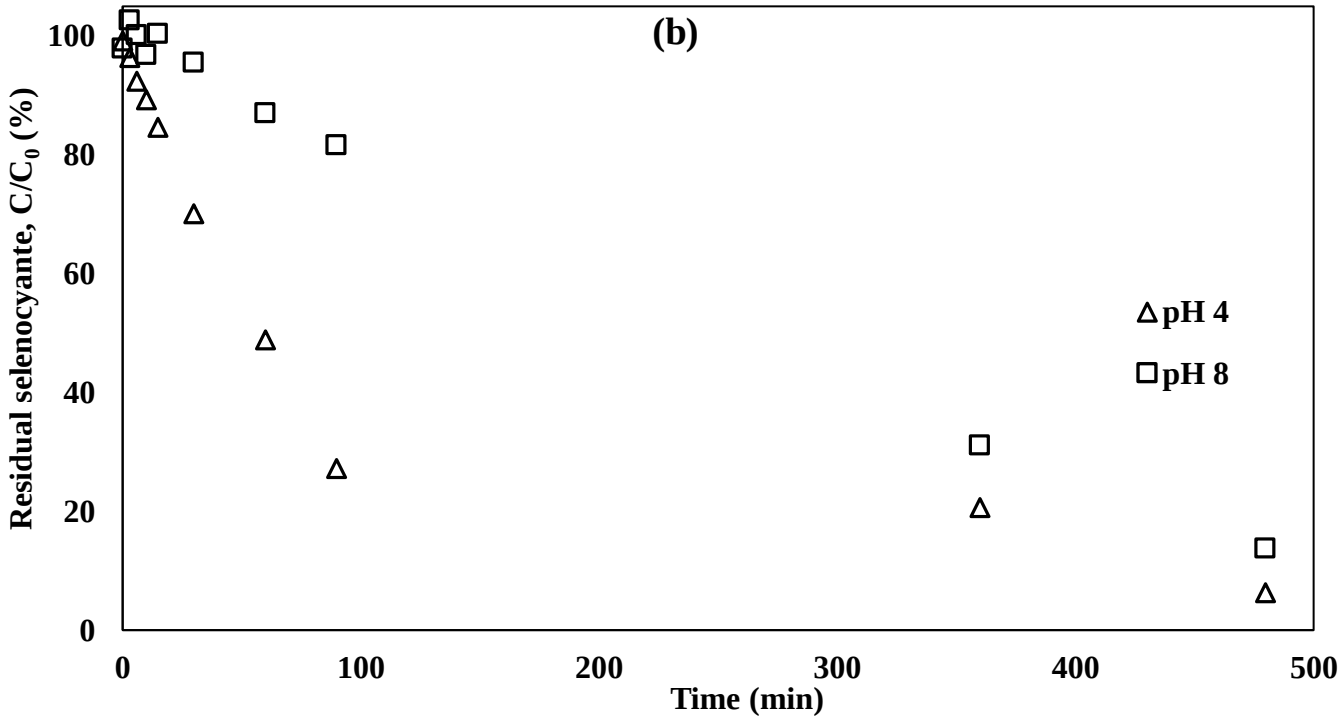

Figure 6. Effect of Initial pH on percentage removal of $SeCN^-$ using steel electrodes at 1.2 A (a) initial concentration of 10 mg/L (b) initial concentration of 50 mg/L.

A qualitatively similar trend was noted for color removal specifically using the steel electrode [21] and for arsenic removal using iron electrode [24-26]. Also as per the classical aqueous speciation chemistry for both iron and aluminum, the precipitation is more conducive in the near neutral pH range, yielding more metal hydroxide species even at lower dissolved metal species concentration, which in turn yields a higher removal of the target pollutant.

3.3. Effect of Current

The effect of current on the removal efficiency of $SeCN^-$ using the steel electrode is shown in **Fig. 7**. The results indicate that the $SeCN^-$ removal efficiency has a direct relation to the magnitude of applied current. This is due to increased dissolution of the anodic electrode at higher current that results in increased metal hydroxide formation yielding enhanced adsorption of $SeCN^-$. In addition, higher current also leads to a faster oxidation of $SeCN^-$ to selenite and selenate which are subsequently removed via adsorption.

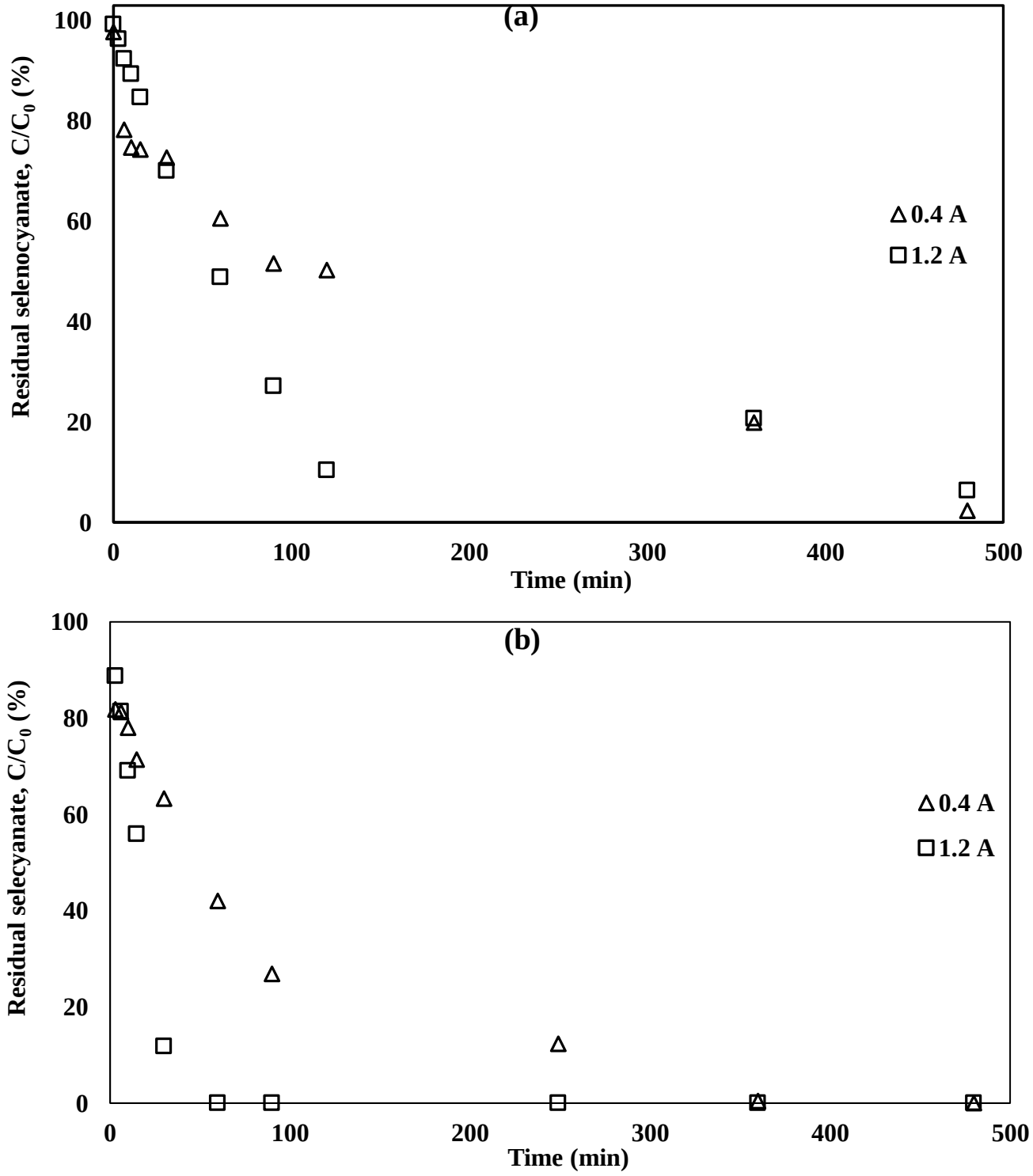

Figure 7. Effect of current on percentage removal of $SeCN^-$ using steel electrodes (a) pH 4, 50 mg/L (b) pH 8, 10 mg/L.

Similar positive effects of applied current on to electrocoagulation process based selenium removal have been noted before as well [2, 21]. Furthermore, Baek et al. [18] who studied electrochemical removal of selenate using iron based anode also noted increased selenate removal at higher current values. The authors suggested reduction of selenate to elemental selenium Se(0) and selenide Se(-II) via ferrous hydroxide that itself oxidized to ferric species. The authors also suggested a

higher formation of ferrous hydroxide at increased current values that in turn caused higher selenate reduction, via ferrous oxidizing to ferric species. The important role of ferrous species was indirectly confirmed, via introduction of higher dissolved oxygen levels that competed with selenate for the ferrous hydroxide species, causing reduced overall selenate removal. Hence the aforementioned higher selenium results as noted in the present study (Fig. 7) at higher current values can also be explained similarly. Furthermore, an increase in the current density also enhances the bubble density along with bubble size reduction [22] that influences the growth and size of flocs formed with positive effects on to pollutants removal efficiency during the electrocoagulation processes [25].

3.4. Effect of Initial Concentration

The initial solution concentration also affects the removal efficiency by influencing the extent of surface and pore coverage of the adsorbent by the adsorbing species. An increase in initial concentration leads to lower removal efficiency as shown in **Fig. 8**. In the first few minutes of the electrochemical process (low charge loading), little quantity of flocs is generated and their pores and surfaces are entirely covered by the various selenium species. Increasing the initial solution concentration implies that more selenium species will be left unadsorbed in the solution phase resulting in a lower removal efficiency. This is clearly seen in **Fig. 8(a)** which shows that at 120 min, about 80% of $SeCN^-$ has been removed from a solution with 10 mg/L initial concentration whereas about 45% removal efficiency has been achieved in a solution with initial $SeCN^-$ concentration of 50 mg/L. The same trend can be observed at a higher current of 1.2 A as shown in **Fig. 8(b)** which shows 100 and 90% removal for 10 and 50 mg/L initial $SeCN^-$ concentration respectively at 120 min. With an increase in the electrochemical time, more flocs are generated which adsorb the selenium species. Nevertheless, on a mass based removal, more selenium removal transpires at high initial selenium. This could result from a higher mass transfer. Though reduction is an important selenium removal mechanism [12] however at higher selenium concentration the chances of interactions between the additional selenocyanate anions and the limited redox species (that are produced during the process) also minimize, thus lowering the overall selenium removal from the respective wastewater streams [15]. This will eventually cause reduced selenium removal from the aqueous phase as well for a fixed treatment duration. Similar concentration effects have been noted previously during electrocoagulation process, nevertheless given sufficient time the process efficiency was noted to be equally matching even at high initial pollutant concentrations [22, 24-25].

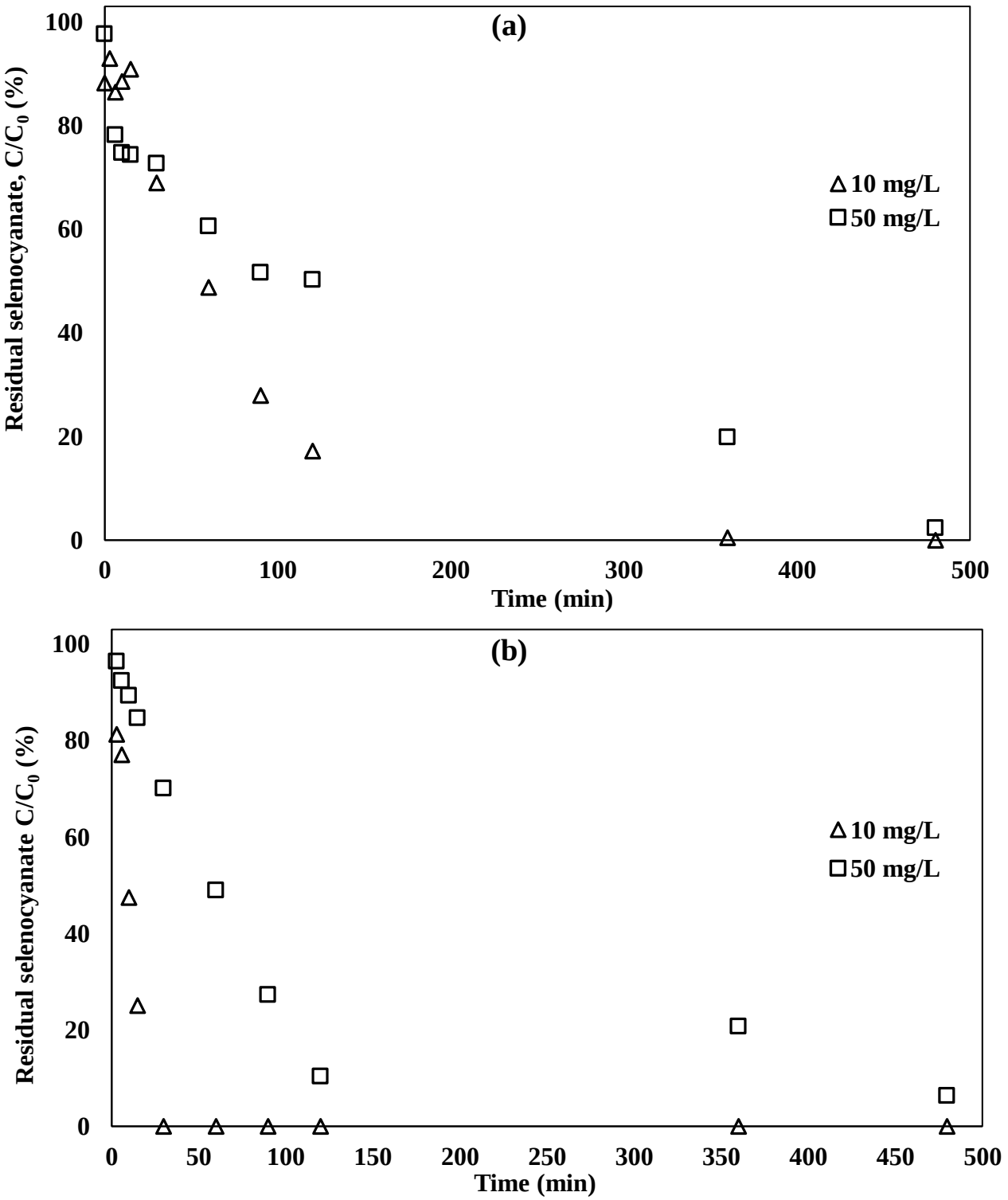

Figure 8. Effect of initial concentration on percentage removal of $SeCN^-$ using steel electrodes at pH 4 (a) 0.4 A (b)1.2 A.

3.5. Kinetic Study

The kinetics of selenocyanate anions removal using the steel, aluminum, graphite, and glassy carbon electrodes was also evaluated at various initial conditions including the initial selenocyanate

anions concentration, pH and applied current. The traditional zero, first and second order rate equations used are given as equations 3, 4 and 5 respectively.

$$C_t = C_0 - k_0 t \quad (3)$$

$$lnC_t = lnC_0 - k_1 t \quad (4)$$

$$\frac{1}{C_t} = \frac{1}{C_0} + k_2 t \quad (5)$$

where k_0 ($mgL^{-1}min^{-1}$), k_1 (min^{-1}) and k_2 ($min^{-1}mg^{-1}L$) are the zero-order, first-order and second-order rate constants respectively that are obtained from the slope of the linear plots of respective equations.

Table 2. Speciation of selenium at various experimental conditions and time intervals.

Electrode	pH	Initial SeCN (mg/L)	Current (A)	Time (min)	% of Initial Se				% of Initial N
					SeCN	SeO_3^{2-}	SeO_4^{2-}	Total Se	Total N
Steel	4	10	0.4	15	90.9	6.9	1.6	99.4	105.0
				30	68.9	5.8	3.2	77.9	84.7
				60	48.8	5.5	4.0	58.4	58.5
				90	28.0	4.3	3.5	35.7	41.9
				360	0.5	1.4	0.9	2.8	18.7
			1.2	15	25.0	50.9	3.5	79.4	28.0
				30	0.0	49.2	28.8	78.0	2.0
				60	0.0	20.4	82.5	102.9	3.5
				90	0.0	0.0	95.3	95.3	4.7
				360	0.0	0.0	5.9	5.9	43.6
		50	0.4	15	74.3	3.7	0.1	78.1	76.0
				30	72.7	5.9	0.3	79.0	74.5
				60	60.6	6.1	0.7	67.5	63.4
				90	51.6	5.8	0.4	57.9	54.1
				360	19.9	2.7	0.1	22.7	24.0
			1.2	15	84.7	1.4	1.2	87.3	91.2
				30	70.1	1.1	1.9	73.2	77.5
				60	48.9	0.5	2.4	51.8	57.1
				90	27.2	0.5	2.5	30.2	35.1
				360	20.7	0.6	0.3	21.6	33.7

Table 2. Speciation of selenium at various experimental conditions and time intervals (continued).

Electrode	pH	Initial SeCN (mg/L)	Current (A)	Time (min)	% of Initial Se				% of Initial N
					SeCN	SeO_3^{2-}	SeO_4^{2-}	Total Se	Total N
Steel	6	10	0.8	15	57.1	11.6	2.0	70.7	73.8

			30	38.8	24.5	2.4	65.6	72.6
			60	8.8	15.0	3.7	27.5	56.6
			90	0.0	15.1	5.8	20.8	77.2
			360	0.1	11.3	2.2	13.6	73.1
	30	0.4	15	87.4	7.7	0.8	95.9	90.3
			30	78.0	7.8	1.3	87.1	80.9
			60	67.4	6.8	2.2	76.4	70.0
			90	54.2	5.7	3.1	63.0	56.6
			360	1.3	4.3	11.5	17.0	4.4
		0.8	15	77.7	11.2	0.8	89.8	82.2
			30	59.3	10.6	2.2	72.1	62.8
			60	32.5	9.9	4.5	46.8	34.9
			90	10.3	5.8	6.0	22.1	12.1
			360	0.6	4.9	4.5	10.0	6.8
		1.2	15	78.8	2.9	3.0	84.7	81.3
			30	62.2	3.5	5.5	71.2	66.2
			60	31.4	3.8	11.8	46.9	36.3
			90	13.5	4.2	16.7	34.3	19.0
			360	1.7	5.6	1.2	8.5	13.4
	50	0.8	15	89.0	2.2	1.0	92.1	92.3
			30	81.6	3.2	1.2	86.0	84.9
			60	65.3	1.9	2.3	69.4	68.1
			90	47.8	2.3	4.1	54.2	50.1
			360	5.2	1.9	3.9	10.9	8.6

Table 2. Speciation of selenium at various experimental conditions and time intervals (continued).

Electrode	pH	Initial SeCN (mg/L)	Current (A)	Time (min)	% of Initial Se				% of Initial N
					SeCN	SeO_3^{2-}	SeO_4^{2-}	Total Se	Total N
	8	10	0.4	15	71.3	17.3	0.9	89.6	86.6
				30	63.3	20.4	1.9	85.6	79.5
				60	42.0	20.8	4.4	67.2	57.9
				90	26.8	18.8	7.3	52.9	42.6
				360	0.4	10.5	16.9	27.7	19.7
			1.2	15	55.9	30.2	10.0	96.0	57.9
				30	11.7	54.2	13.6	79.5	13.6
				60	0.0	25.8	31.7	57.5	3.3
				90	0.0	12.7	38.5	51.2	4.5
				360	0.0	6.1	48.3	54.4	41.8
		50	0.4	15	100.4	4.0	0.1	104.5	102.5
				30	95.5	3.4	0.3	99.2	97.6
				60	87.0	3.6	0.7	91.3	90.8
Steel				90	81.7	1.5	1.3	84.5	85.1

			1.2	360	31.1	3.3	6.0	40.4	35.6
				15	85.2	8.0	3.9	97.2	85.2
				30	75.8	13.5	6.4	95.7	76.7
				60	52.9	17.9	13.1	83.9	53.4
				90	32.4	12.0	19.2	63.7	32.5
				360	2.6	6.9	22.7	32.3	8.9

Table 2. Speciation of selenium at various experimental conditions and time intervals (continued).

Electrode	pH	Initial SeCN (mg/L)	Current (A)	Time (min)	% of Initial Se				% of Initial N
					SeCN	SeO_3^{2-}	SeO_4^{2-}	Total Se	Total N
Aluminum	4	10	0.4	15	91.2	7.1	0.1	98.4	94.2
				30	90.8	5.5	0.3	96.5	94.6
				60	89.8	3.5	0.1	93.4	94.6
				90	86.5	3.4	0.1	89.9	90.9
				360	77.5	2.5	0.1	80.1	82.6
			0.8	15	95.6	3.6	0.1	99.3	96.3
				30	98.3	7.7	0.0	105.9	99.8
				60	97.5	10.1	0.1	107.7	98.8
				90	93.6	7.2	0.0	100.9	95.3
				360	46.1	5.3	0.0	51.4	48.2
			1.2	15	90.2	0.9	0.0	91.1	96.8
				30	90.5	0.7	0.0	91.2	98.1
				60	89.3	1.8	0.0	91.2	96.0
				90	86.1	2.4	0.0	88.5	92.9
				360	8.7	3.3	0.0	12.0	13.2
		50	1.2	15	97.5	0.6	0.0	98.1	97.4
				30	97.0	0.5	0.0	97.5	96.8
				60	96.5	0.3	0.0	96.8	96.6
				90	101.7	0.2	0.0	101.9	101.5
				360	89.0	1.4	0.0	90.4	89.1
	8	10	1.2	15	95.2	2.9	0.0	98.1	97.8
				30	92.4	3.0	0.0	95.5	95.6
				60	90.4	3.0	0.0	93.5	93.6
				90	88.0	2.1	0.0	90.1	93.1
				360	64.5	7.2	0.3	71.9	69.2
		50	1.2	15	99.5	0.9	0.0	100.4	100.9
				30	100.3	1.0	0.0	101.3	101.8
				60	97.9	1.0	0.0	98.8	99.4
				90	97.2	1.9	0.0	99.1	98.6
				360	99.5	1.5	0.0	100.9	100.9

Table 2 shows the time-dependent concentration various for various reaction intermediates formed during the electrocoagulation process while Table 3 shows the kinetic parameters for the three models used. Among the three kinetic models considered, the first-order model suitably described the kinetics as represented by the R^2 while the zero-order model is the least suitable. It can be observed that keeping the same experimental conditions, the rate constant value is decreased as the initial concentration of the selenocyanate anions in the aqueous solution is increased. The aforementioned discussion on the effect of pollutant concentration onto electrocoagulation process efficiency (section 3.4) along with factors such as the pollutant mass transfer limitations from the bulk phase to the metal hydroxide surface can explain the respective trends.

Table 3. Kinetic parameters of selenocyanate anions removal in the electrocoagulation process.

Electrode	Conc. (mg/L)	Current (A)	pH	Zero-order		First-order		Second-order	
				k_0 (mg L^{-1} min^{-1})	R^2	k_1 (min^{-1})	R^2	k_2 (L mg^{-1} min^{-1})	R^2
Steel	50	1.2	8	0.137	0.728	0.010	0.970	0.002	0.937
	10	1.2	8	0.023	0.377	0.071	0.938	0.026	0.838
	10	1.2	4	0.019	0.293	0.090	0.940	0.020	0.861
	50	1.2	4	0.084	0.614	0.005	0.710	0.001	0.705
	30	1.2	6	0.054	0.586	0.010	0.876	0.006	0.987
	50	0.4	4	0.084	0.812	0.006	0.910	0.001	0.677
	10	0.4	4	0.025	0.734	0.015	0.997	0.058	0.878
	50	0.4	8	0.098	0.953	0.004	0.900	0.000	0.781
	10	0.4	8	0.030	0.834	0.013	0.926	0.043	0.669
	30	0.4	6	0.088	0.942	0.010	0.812	0.004	0.660
	50	0.8	6	0.107	0.841	0.007	0.963	0.001	0.927
	10	0.8	6	0.116	0.920	0.037	0.976	0.014	0.877
	30	0.8	6	0.097	0.591	0.016	0.791	0.014	0.896
Aluminum	10	1.2	7.95	0.007	0.945	0.001	0.940	0.000	0.931
	10	1.2	3.98	0.021	0.895	0.009	0.807	0.030	0.558
	50	1.2	4.02	0.015	0.633	0.000	0.647	0.000	0.658
	10	0.4	4.02	0.005	0.937	0.001	0.922	0.000	0.897
	10	0.8	4.03	0.016	0.851	0.003	0.797	0.001	0.698
Graphite	50	1.2	8.19	0.139	0.617	0.012	0.942	0.003	0.943
Glassy Carbon	10	1.2	3.98	0.016	0.840	0.004	0.972	0.001	0.993

This is due to the reduced rate of selenocyanate anions removal associated with decreasing ratio of the dissolved anode species to the initial solution concentration.

3.6. Sludge Characterization

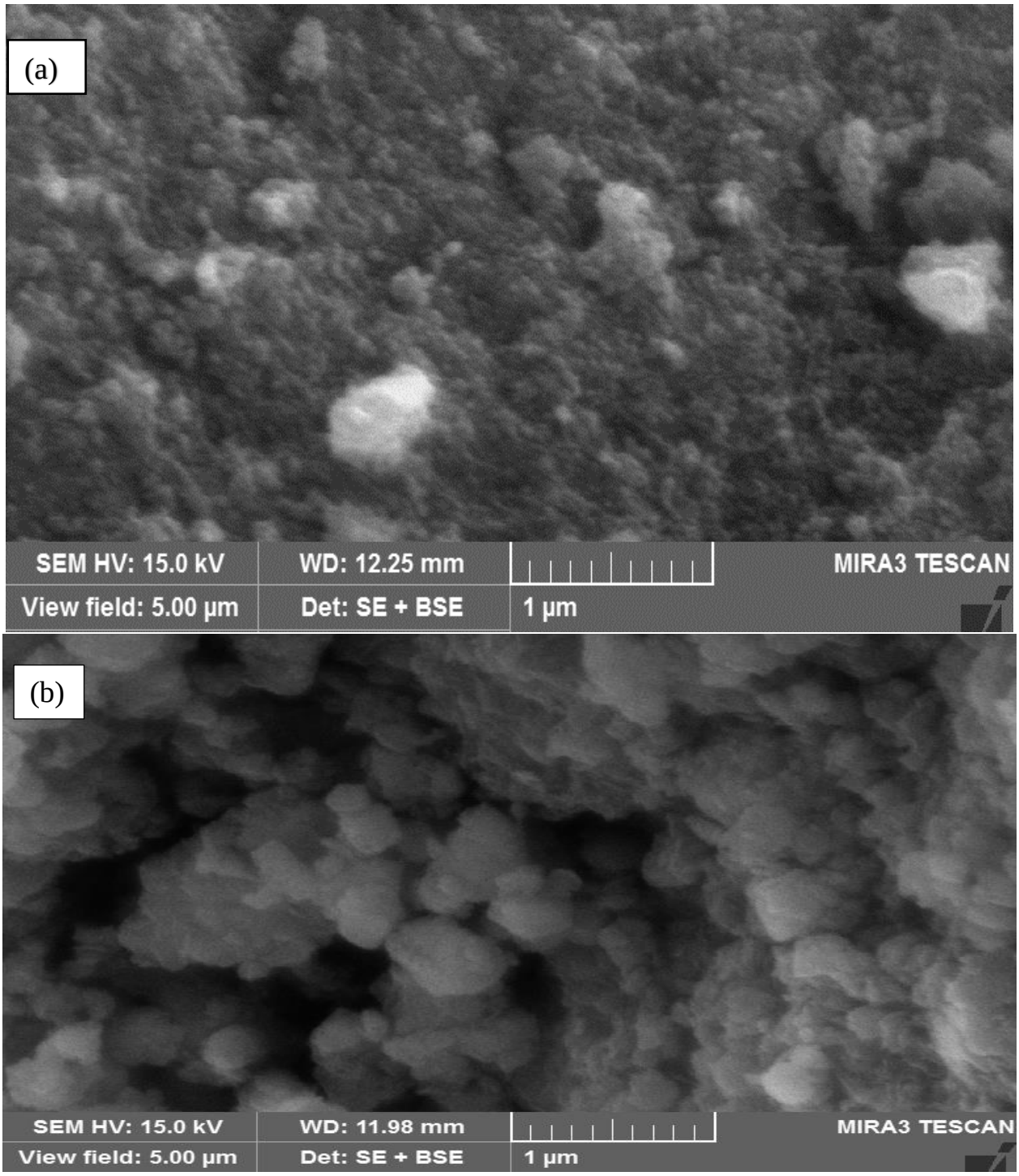

Figure 9. SEM images of sludge obtained from the electrocoagulation process of $SeCN^-$ removal (a) steel electrode (b) aluminum electrode.

The surface morphology of sludge obtained from the steel and aluminum electrodes is shown in **Fig. 9**. The SEM images show a rough agglomeration of the particles, which are typically non-uniformly distributed at the surface of precipitates.

Table 4. EDX analysis of the elemental composition of the electrocoagulation sludge.

	Steel electrodes		Al electrodes	
Elements	Weight %	Atomic %	Weight %	Atomic %
C	9.26	17.43	34.13	43.64
O	45.06	63.69	48.99	47.03
Cl	1.22	0.78	0.66	0.29
Cr	8.53	3.71	------	------
Fe	32.01	12.96	------	------
Ni	3.22	1.24	------	------
Se	0.70	0.20	0.25	0.05
Al	------	------	15.65	8.91

This may be due to coagulation and adsorption of selenium species along with other particles present in the aqueous medium. Moreover, the EDX analysis contained in **Table 4** confirms the presence of selenium, along with other elements in the sludge, indicating selenium removal during the electrocoagulation process. The EDX analysis of the respective sludge (Table 3) reveals that the surface atomic ratio of Se/Fe is 0.0154 which is almost three times that of Se/Al (0.0056).

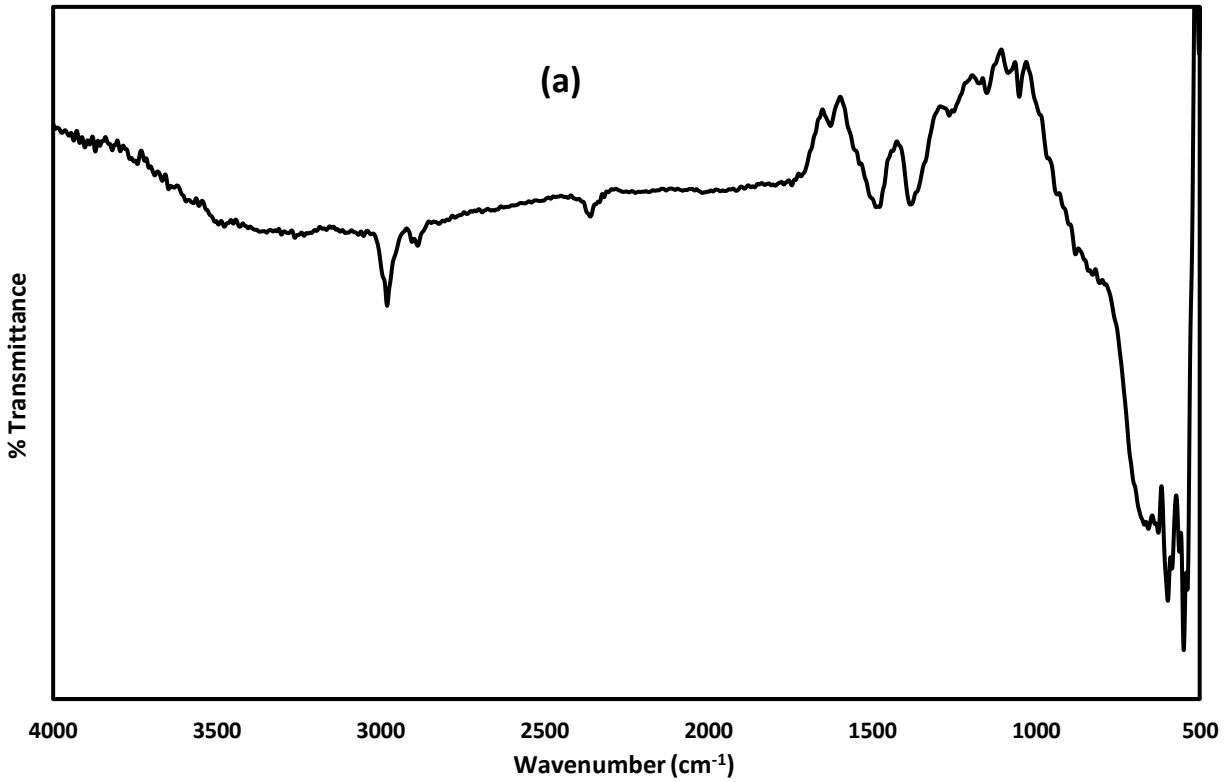

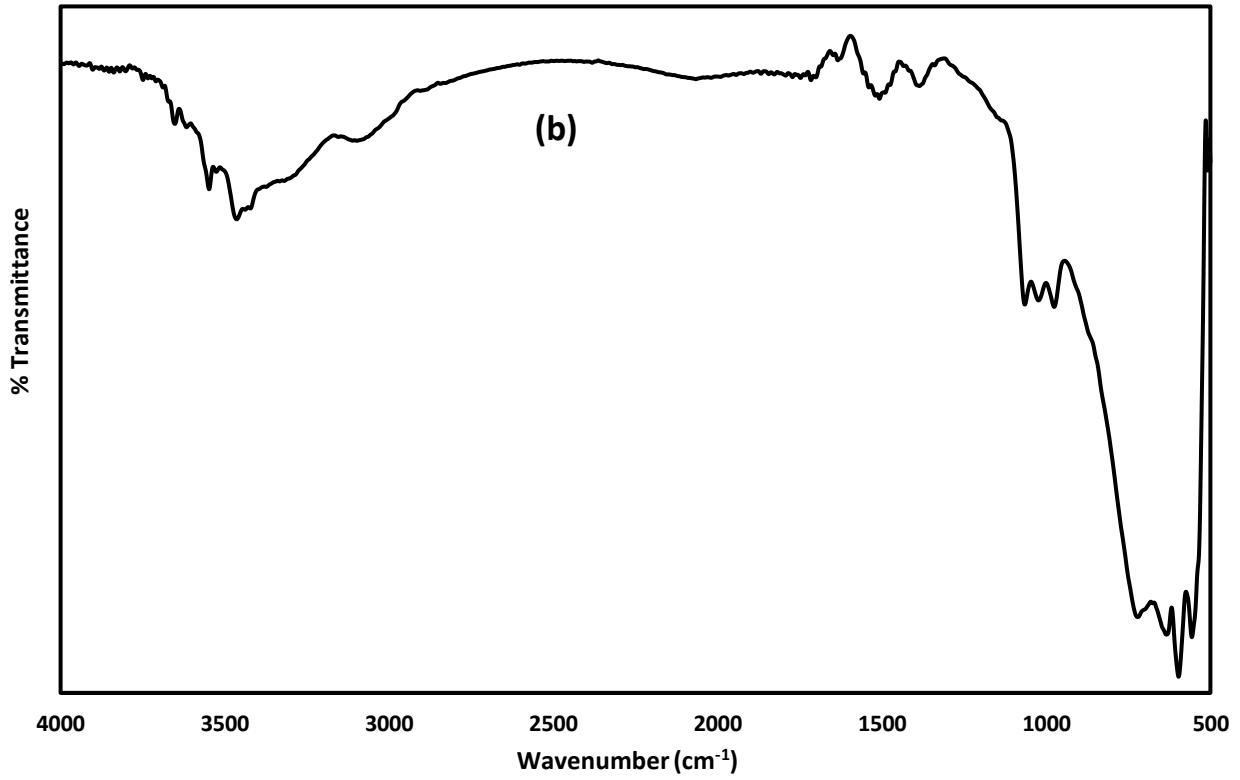

Figure 10. FTIR images of sludge obtained from the electrocoagulation process of $SeCN^-$ removal (a) steel electrode (b) aluminum electrode.

This further confirms the superior adsorption capacity of iron hydroxide as compared with aluminum hydroxide for selenium removal as previously discussed. Manceau and Gallup [11] also report treatment of selenocyanate containing wastewaters using copper (II) salts and via precipitation. The authors investigated the form in which selenocyanate based selenium was eventually removed. Employing the XANES (X-ray absorption near-edge structure) and EXAFS (extended X-ray absorption fine structure) spectroscopy techniques, the selenium species was noted to be bound with copper thiocyanate. The selenium was also noted to be present as selenide linked to C and Cu atoms. The respective findings from the treatment of selenocyanate containing wastewater streams also indicate incorporation of selenium species into the sludge formed during the reduction/precipitation process. The aforementioned findings from the present work (Table 3) that showed a surface Se/Fe atomic ratio of 0.0154 also support incorporation of selenium into iron anode produced sludge during the electrocoagulation process. These findings thus suggest that adsorption, redox reactions, and surface incorporation of resulting selenium species during electrocoagulation process, initiate the removal of selenium.

Fig. 10 shows the FTIR spectra of the sludge obtained using steel and aluminum electrodes. The OH stretching vibrations indicating the hydroxyl groups are located at 3340 cm^{-1} while hydroxyl (OH) bending vibrations are located at 1635 cm^{-1} [26]. The band at 2359 cm^{-1} in Fig. 10(a) is conspicuously missing in Fig. 10(b). This band is associated with the stretching vibration of CN of $SeCN^-$. The observation suggests the removal of $SeCN^-$ by the steel electrode while negligible quantity was removed by the aluminum electrode.

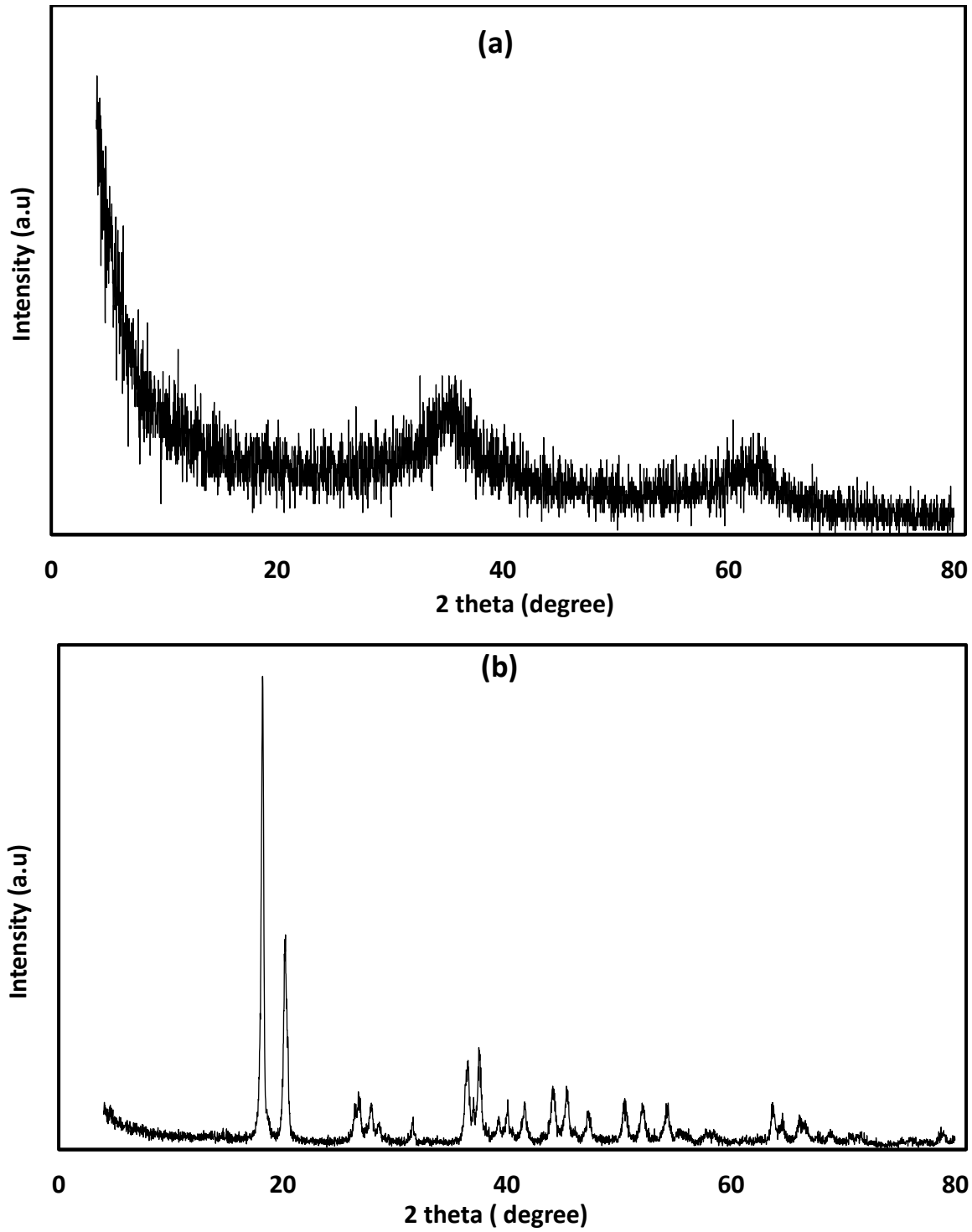

Figure 11 XRD of sludge obtained in the electrocoagulation process of selenocyanate anions removal (a) steel electrode (b) aluminum electrode.

Fig. 11a and 11b show the XRD diffractograms of the sludge produced during the electrocoagulation process. The steel sludge (Fig. 11 (a)) contains predominantly amorphous phase while Fig.11 (b) indicates the presence of predominantly $Al(OH)_3$ phase according to the JCPDS (01-070-2038). The phases associated with the selenium species are not sharp due to the relatively low concentration of the solution used in the study.

3.7. Molecular Level Simulations

A molecular-level simulation was also performed to study the interactions of various hydroxides of iron and aluminum with varying concentrations of selenite and selenite species. In this study, the respective interaction processes between the selenite and selenate present in the solution with the hydroxides of the aluminum and iron electrodes material were simulated and studied using molecular simulations technique which is based on molecular mechanics (MM), molecular dynamics (MD) and Monte Carlo (MC) interactions (Details in the Materials and Methods).

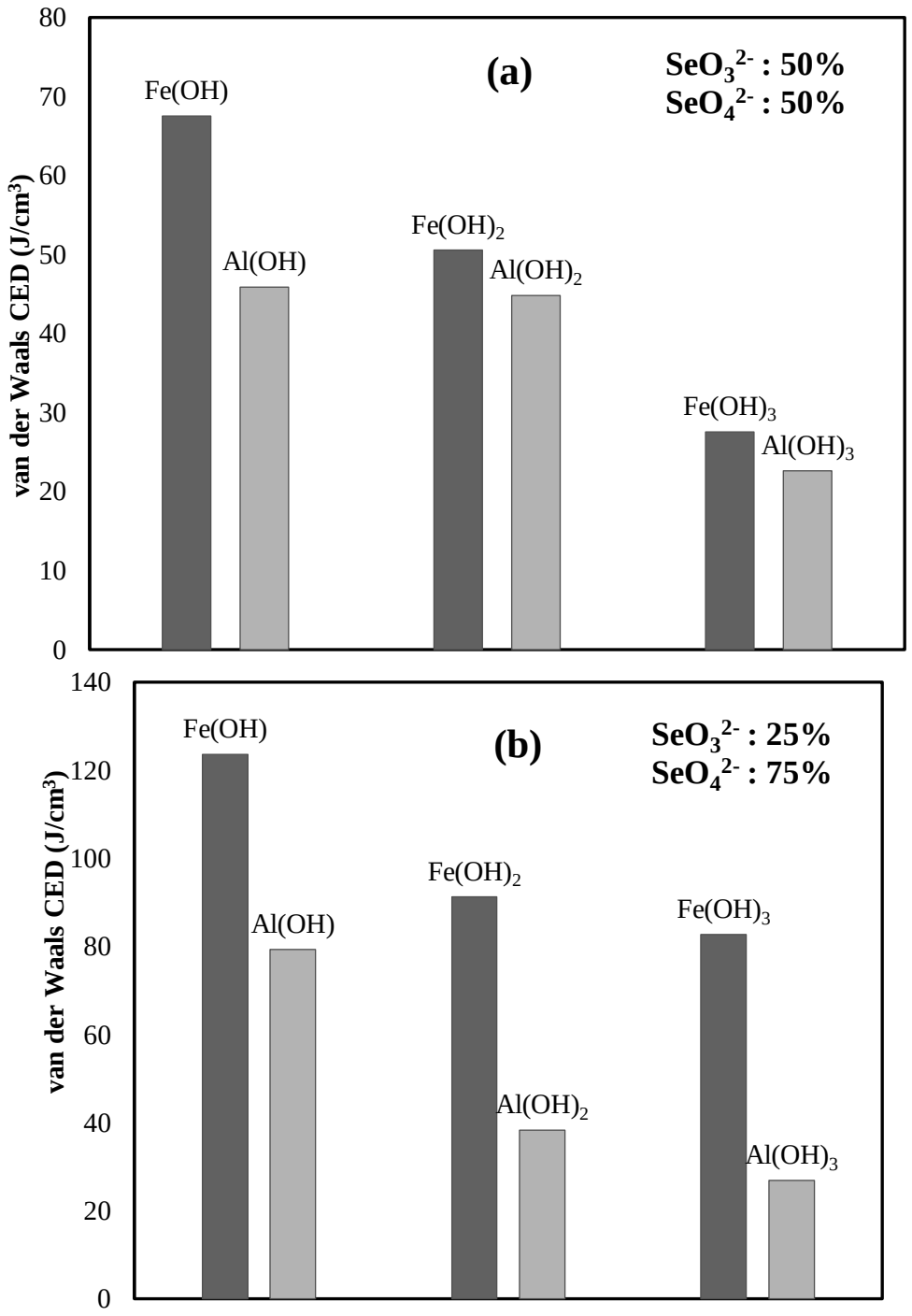

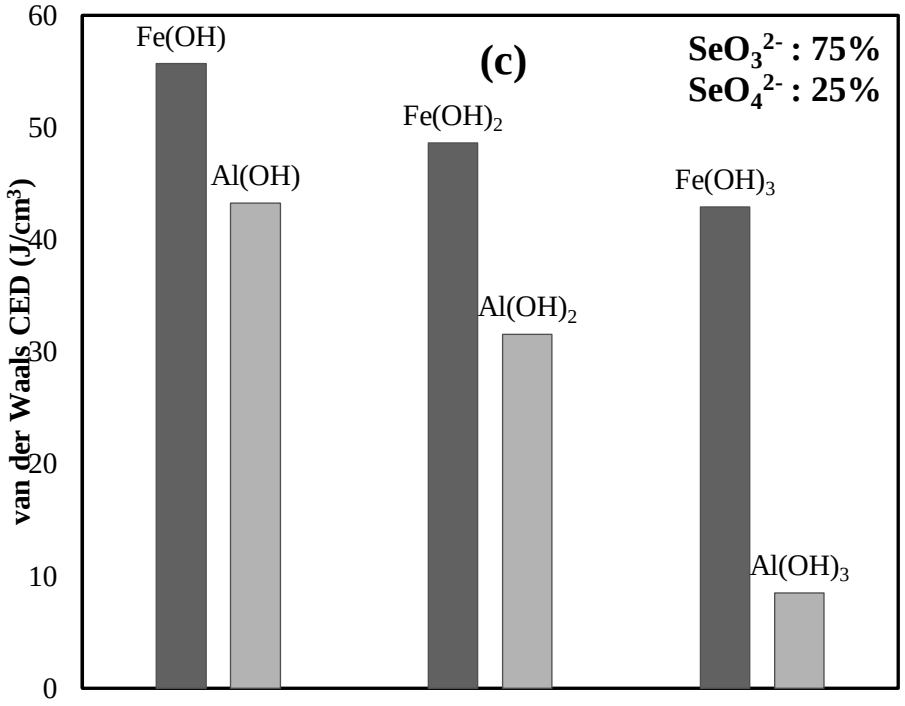

Figure 12. Van der Waals cohesive energy density (CED) comparison for aluminum and iron hydroxides interactions with various concentrations of selenite and selenate (a) 50% SeO_3^{2-}, 50% SeO_4^{2-} (b) 25% SeO_3^{2-}, 75% SeO_4^{2-} (c) 75% SeO_3^{2-}, 25% SeO_4^{2-}

The cohesive energy density (CED) and its components (electrostatic and van der Waals) play a vital role in understanding the various processes involving binding/attraction/cohesiveness in any typical molecular system [27-30]. Quantitatively, CED is the amount of energy needed for the transition of a mole of material from the liquid to the gaseous phase and is considered as a measure of the mutual attractiveness of the molecules. As CED concept is quite analogous to the flocculation processes controlling the removal of selenium, it has found to be sensitive to all these possible interactions at the molecular level. Both the components of CED i.e. electrostatic and van der Waals, of the simulated mixes were determined by the Forcite module of the Materials Studio software.

Using the variation of the van der Waals CED with various interactions, the corresponding plots were prepared for various hydroxides of iron and aluminum and the selenite and selenite species (**Fig. 12**). These plots generally show a decrease in van der Waals CED with an increase in $(OH)_x$ group, both for iron and aluminum. Moreover, it could be observed from these plots that iron hydroxides have higher CED as compared to their aluminum counterparts which also supports our aforementioned selenium removal results using the steel electrode that showed higher efficiency compared to the aluminum electrode. Based on these results, van der Waals CED could be considered as a direct indicator of the attraction/flocculation of the selenium oxides with the electrode hydroxides.

4. CONCLUSIONS

This work explored the application of electrocoagulation process for the treatment of selenocyanate anions ($SeCN^-$) contaminated wastewater. The effect of electrode type, pH, applied

current and initial concentration on to $SeCN^-$ removal efficiency were evaluated. The $SeCN^-$ removal efficiency increased with an increase in the applied current and reaction time but decreased at higher pH and selenium concentration. During the electrocoagulation process, the $SeCN^-$ complex destruction was followed by oxidation to selenite and selenate and subsequent removal of the respective selenium species by the anode generated flocs. It was also observed that the coagulant generated using the steel electrode was more effective for SeO_3^{2-}/SeO_4^{2-} removal from the aqueous solution as compared to the coagulant produced using the aluminum electrode. The glassy carbon and graphite electrodes only converted the $SeCN^-$ to other selenium species without their removal (because of no coagulant production), hence leading to accumulation of selenite and selenate in the aqueous medium. The zeta potential measurement of the flocs produced during the EC process transited from positive at low pH to negative at higher pH. Subsequently, the anionic selenite/selenate species showed high adsorption-based removal at low pH and least removal at high pH. The sludge characterization using the SEM, EDX, XRD, and FTIR confirmed the adsorption of selenium onto the surface of flocs generated during the electrocoagulation process as well as superior adsorption tendency of iron hydroxide for selenium when compared to aluminum hydroxide. This was further validated by the van der Waals CED computation where iron hydroxide showed higher CED values in comparison to aluminum hydroxides. In summary, the results from the present work indicate that the EC technique under appropriate process condition can be successfully used for the treatment of $SeCN^-$ contaminated wastewater along with the removal of selenium intermediates via adsorption.

ACKNOWLEDGEMENT
The authors acknowledge the Civil and Environmental Engineering department at KFUPM and express their heartfelt gratitude for providing the laboratory facilities for this research.

References

1. V. Vimonses, S. Lei, B. Jin, C.W. Chow, C. Saint, Chemical Engineering Journal, 148 (2009) 354.
2. H.K. Hansen, S.F. Peña, C. Gutiérrez, A. Lazo, P. Lazo, L.M. Ottosen, Journal of Hazardous Materials, 364 (2019) 78.
3. N. Hadrup, K. Loeschner, K. Skov, G. Ravn-Haren, E.H. Larsen, A. Mortensen, H.R. Lam, H.L. Frandsen, PeerJ, 4 (2016) e2601.
4. W. Maher, A. Roach, M. Doblin, T. Fan, S. Foster, R. Garrett, G. Möller, L. Oram, D. Wallschläger, Environmental sources, speciation, and partitioning of selenium, in: Ecological assessment of selenium in the aquatic environment, CRC Press, 2010, pp. 63-108.
5. X. Meng, S. Bang, G.P. Korfiatis, Water Research, 36 (2002) 3867.
6. R. Lukasiewicz, Selenium speciation of process and discharge waters by IC-ICP-MS, in: Winter Conference on Plasma Spectrochemistry, San Diego, CA, 1994.
7. E.D. Van Hullebusch, Bioremediation of Selenium contaminated wastewater, Springer, 2017.
8. G.B. Tonietto, J.M. Godoy, A.C. Oliveira, M.V. de Souza, Analytical and Bioanalytical chemistry, 397 (2010) 1755.
9. W. Coleman, C. McCrosky, Journal of the American Chemical Society, 59 (1937) 1458.
10. K.L. LeBlanc, M.S. Smith, D. Wallschläger, Environmental Science & Technology, 46 (2012) 5867.
11. A. Manceau, D.L. Gallup, Environmental Science & Technology, 31 (1997) 968.
12. Y. Nancharaiah, M. Sarvajith, P. Lens, Water Research, 131 (2018) 131.

13. R. Burra, J.D. Fox, G.A. Pradenas, C.C. Vásquez, T.G. Chasteen, Environmental Technology, 30 (2009) 1327.
14. B.A. Labaran, M.S. Vohra, CLEAN–Soil, Air, Water, 45 (2017) 1600268.
15. B.A. Labaran, M.S. Vohra, Environmental Technology, 35 (2014) 1091.
16. M.S. Vohra, Fresenius Environmental Bulletin, 24 (2015) 1108.
17. B.A. Labaran, M.S. Vohra, Desalination and Water Treatment, 124 (2018) 267.
18. K. Baek, N. Kasem, A. Ciblak, D. Vesper, I. Padilla, A.N. Alshawabkeh, Chemical Engineering Journal, 215-216 (2013) 678.
19. P.R. Kumar, S. Chaudhari, K.C. Khilar, S. Mahajan, Chemosphere, 55 (2004) 1245.
20. Z. Murthy, S. Parmar, Desalination, 282 (2011) 63.
21. M.K.N. Mahmad, M.M.R. Rozainy, I. Abustan, N. Baharun, Procedia Chemistry, 19 (2016) 681.
22. E. Bazrafshan, K.A. Ownagh, A.H. Mahvi, Journal of Chemistry, 9 (2012) 2297.
23. E. Bazrafshan, A.H. Mahvi, S. Naseri, A.R. Mesdaghinia, Turkish Journal of Engineering and Environmental Sciences, 32 (2008) 59.
24. W. Wan, T.J. Pepping, T. Banerji, S. Chaudhari, D.E. Giammar, Water research, 45 (2011) 384.
25. M. Kobya, U. Gebologlu, F. Ulu, S. Oncel, E. Demirbas, Electrochimica Acta, 56 (2011) 5060.
26. J.R. Parga, D.L. Cocke, J.L. Valenzuela, J.A. Gomes, M. Kesmez, G. Irwin, H. Moreno, M. Weir, Journal of Hazardous Materials, 124 (2005) 247.
27. H. Ahmed, S. Abduljauwad, Geotechnique, 67 (2016) 187.
28. H. Ahmed, S. Abduljauwad, Journal of Natural Gas Science and Engineering, 48 (2017) 85.
29. H. Ahmed, S. Abduljauwad, Arabian Journal of Geosciences, 10 (2017) 448.
30. H. Ahmed, in, PhD dissertation, Civil Engineering Department, King Fahd University of Petroleum & Minerals, 2015.